Atmospheric
Chemistry
and Physics
Discussions

Impact of El Niño Southern Oscillation on the interannual variability of methane and tropospheric ozone.

Matthew J. Rowlinson[1], Alexandru Rap[1], Stephen R. Arnold[1], Richard J. Pope[1,2], Martyn P. Chipperfield[1,2], Joe McNorton[3], Piers Forster[4], Hamish Gordon[1], Kirsty J. Pringle[1], Wuhu Feng[1,5], Brian J. Kerridge[6,7], Barry L. Latter[6,7], Richard Siddans[6,7]

[1]Institute for Climate and Atmospheric Science, School of Earth and Environment, University of Leeds, Leeds, LS2 9JT, UK
[2]National Centre for Earth Observation, University of Leeds, Leeds, LS2 9JT, UK
[3]European Centre for Medium-Range Weather Forecasts, Reading, RG2 9AX, UK
[4]Priestley International Centre for Climate, University of Leeds, LS2 9JT, Leeds, UK
[5]National Centre for Atmospheric Science, University of Leeds, LS2 9JT, Leeds, UK
[6]Remote Sensing Group, STFC Rutherford Appleton Laboratory, Harwell, Oxfordshire, UK
[7]National Centre for Earth Observation, Harwell, Oxfordshire, UK

Correspondence to: Matthew J. Rowlinson (ee11mr@leeds.ac.uk)

Atmospheric
Chemistry
and Physics
Discussions

Abstract. The growth rate of global methane (CH_4) concentrations has a strong interannual variability which is believed to be driven largely by fluctuations in CH_4 emissions from wetlands and wildfires, as well as changes to the atmospheric sink. The El Niño Southern Oscillation (ENSO) is known to influence fire occurrence, wetland emission and atmospheric transport, but there are still important uncertainties associated with the exact mechanism and magnitude of this influence. Here we use a modelling approach to investigate how fires and meteorology control the interannual variability of global carbon monoxide (CO), CH_4 and ozone (O_3) concentrations, particularly during large El Niño events. Using a three-dimensional chemical transport model (TOMCAT) coupled to a sophisticated aerosol microphysics scheme (GLOMAP) we simulate changes to CO, hydroxyl radical (OH) and O_3 for the period 1997-2014. We then use an offline radiative transfer model to quantify the impact of changes to atmospheric composition as a result of specific drivers.

During the El Niño event of 1997-1998, there were increased emissions from biomass burning globally. As a result, global CO concentrations increased by more than 40%. This resulted in decreased global mass-weighted tropospheric OH concentrations of up to 9% and a resulting 4% increase in the CH_4 atmospheric lifetime. The change in CH_4 lifetime led to a 7.5ppb yr^{-1} increase in global mean CH_4 growth rate in 1998. Therefore biomass burning emission of CO could account for 72% of the total effect of fire emissions on CH_4 growth rate in 1998.

Our simulations indicate variations in fire emissions and meteorology associated with El Niño have opposing impacts on tropospheric O_3 burden. El Niño-related atmospheric transport changes decrease global tropospheric O_3 concentrations leading to a -0.03 Wm^{-2} change in O_3 radiative effect (RE). However, enhanced fire emission of precursors such as nitrous oxides (NO_x) and CO increase O_3 RE by 0.03 Wm^{-2}. While globally the two mechanisms nearly cancel out, causing only a small change in global mean O_3 RE, the regional changes are large – up to -0.33 Wm^{-2} with potentially important consequences for atmospheric heating and dynamics.

1 Introduction

70   In terms of radiative forcing, methane (CH_4) is the second most important anthropogenically emitted greenhouse gas after CO_2 (Myhre et al., 2013). Concentrations of CH_4 have risen from approximately 722 ppb in 1750 to over 1850 ppb in 2018, an increase of more than 150% (Dlugokencky, 2019). During this time period CH_4 has contributed an estimated radiative forcing (RF) of 0.48 ± 0.05 Wm^{-2}, around 20% of the total direct anthropogenic RF from greenhouse gases (Myhre et al., 2013). Furthermore, CH_4 is a precursor of tropospheric ozone (O_3), which is also a greenhouse gas responsible for RF of 0.4 ± 0.2

75   Wm^{-2} since the pre-industrial (Myhre et al., 2013), as well as a harmful pollutant that damages human health (Anenberg et al., 2010) and ecosystems (Sitch et al., 2007). While anthropogenic emissions have driven the long-term increase in CH_4 concentrations, CH_4 is also emitted from a range of natural sources leading to strong interannual variability (IAV) (Bousquet et al., 2006; Dlugokencky et al., 2011; Nisbet et al., 2016). Understanding the mechanisms driving IAV is important for accurate predictions of future CH_4 concentrations, especially in the context of anthropogenic emission reductions.

80   Previous studies indicate that although anthropogenic sources may contribute to seasonal variations in atmospheric CH_4, natural sources are the primary drivers of IAV (Bousquet et al., 2006; Meng et al., 2015). Emissions from natural wetlands have been shown to be the dominant process, with emissions from fires and changes to the atmospheric sink also playing important roles (Bousquet et al., 2006; Chen and Prinn, 2006; Dlugokencky et al., 2011; Kirschke et al., 2013; McNorton et al., 2016; Corbett et al., 2017). These natural sources are climate sensitive, so interannual changes to temperature and

85   precipitation affect the amount of CH_4 emitted into the atmosphere as well as the spatial distribution (Zhu et al., 2017). Studies have found that biomass burning emissions are largely responsible for the IAV of carbon monoxide (CO) and also affect O_3 concentrations (Granier et al., 2000; Monks et al., 2012; Voulgarakis et al., 2015). Although Szopa et al. (2007) found meteorology is a more important driver of IAV for CO, explaining 50-90% of IAV.

A major driver of climatic IAV is the El Niño Southern Oscillation (ENSO) – a mode of climate variability originating in the

90   Pacific Ocean with alternating warm (El Niño) and cold (La Niña) modes (McPhaden et al., 2006). Positive phase El Niño events lead to warmer and drier conditions in much of the tropics, disrupting global circulation patterns and leading to widespread changes in fire occurrence, wetland emissions and atmospheric transport (Feely et al., 1987; Jones et al., 2001; McPhaden et al., 2006). These influences occur most strongly in the tropics but have global consequences (Jones et al., 2001). Global CH_4 concentrations have been observed to increase significantly during El Niño events, with an especially strong signal

95   during the 1997-1998 event when the CH_4 growth rate was 12 ppb yr^{-1}, almost triple the 1750-2018 mean annual growth rate (Rigby et al., 2008; Hodson et al., 2011). Due to the wide-ranging effects of El Niño and varied sources of CH_4, there are multiple factors which could trigger the increase in CH_4 growth rate. Chen and Prinn (2006) attributed the increase to anomalies in global wetland emissions; however Zhu et al. (2017) estimated that although 49% of the interannual variation in wetland emissions can be explained by ENSO, wetland emissions were significantly lower during El Niño including the 1997-1998

100   event. Bousquet et al. (2006) suggested that the increased CH_4 growth rate during the 1997-1998 El Niño was primarily caused by abnormally large peat fires in Indonesia emitting huge amounts of CH_4 while wetlands emissions remained stable (van der Werf et al., 2004; Butler et al., 2005; Bousquet et al., 2006).

In addition to direct emissions of CH_4 from fires, it has been proposed that anomalously large CO emissions during enhanced El Niño fire events could explain the changes to CH_4 growth rate (Butler et al., 2005; Bousquet et al., 2006). CO is emitted

105   from biomass burning in much larger quantities than CH_4 (~20x larger) and its reaction with the hydroxyl radical (OH) is its primary atmospheric sink (Voulgarakis and Field, 2015). Abnormal increases in CO concentrations may suppress the availability of OH, thereby extending CH_4 lifetime and increasing its growth rate during and following large fire events (Butler et al., 2005; Manning et al., 2005). The reaction of CH_4 with OH is the largest term in the global CH_4 budget, accounting for ~90% of its sink (McNorton et al., 2016), therefore even minor changes to OH caused by the presence of other compounds or changes to atmospheric transport and photolysis rates could have a large impact on CH_4 growth rate (Dlugokencky et al., 2011).

110

Butler et al. (2005) found that CO emissions suppressed OH concentrations by 2.2% in 1997-1998, which accounted for 75% of the observed change in CH_4 concentration. Bousquet et al. (2006) also reported a weakened OH sink during this El Niño event.

Here we use a modelling approach to investigate how El Niño events affect global CH_4, CO and tropospheric O_3 concentrations through changes to fire occurrence and atmospheric transport. Using long-term simulations spanning multiple El Niño and La Niña events, we quantify the relative influence of changes to fire emissions and dynamical transport. We also differentiate between the effect of direct CH_4 emissions from fires and the indirect effect via CO emissions and atmospheric chemistry changes.

2 Models and Simulations

2.1 Model description

For this study we use the TOMCAT chemical transport model (Chipperfield, 2006) coupled to the GLOMAP global aerosol microphysics scheme (Mann et al., 2010). The version of TOMCAT-GLOMAP used here is a further development of the version described by Monks et al. (2017). Cloud fields are now provided from the European Centre for Medium-Range Weather Forecasts (ECMWF) reanalyses (Dee et al., 2010), replacing the climatological clouds fields used previously from the International Satellite Cloud Climatology Project (ISCCP) (Rossow and Schiffer, 1999), leading to improved representation of photolysis. Other developments include updated emission inventories, the inclusion of CERN CLOUD-based new particle formation and the introduction of Martensson sea spray emissions (Gordon et al., 2017; Monks et al., 2017). The model is run at 2.8° x 2.8° horizontal resolution with 31 vertical levels, driven by 6-hourly ECMWF ERA-Interim reanalyses. The planetary boundary layer (PBL) scheme is based on Holtslag and Boville (1993) and sea surface temperatures are from ECMWF reanalyses.

The tropospheric chemistry scheme used is as described in Monks et al. (2017) with anthropogenic emissions from the Monitoring Atmospheric Composition and Climate (MACCity) emissions inventories (Lamarque et al., 2010). Annually varying emission inventories are included for all fire-emitted gas-species, aerosol emissions such as black carbon (BC) and all sources of CH_4. The Global Fire Emissions Database (GFED) used by TOMCAT-GLOMAP has been updated to version 4 with CO, nitrous oxides (NO_x) and volatile organic compound (VOC) emissions from fires (Randerson et al., 2017; Reddington et al., 2018). Biogenic emissions are taken from MACCity and CCMI (Chemistry-Climate Model Initiative: http://www.met.reading.ac.uk/ccmi/). The CH_4 inventory is provided from a new emissions inventory derived from the Joint UK Land Environment Simulator (JULES), combined with biomass burning emissions from GFEDv4 (McNorton et al., 2016; Randerson et al., 2017). Surface CH_4 concentrations are scaled annually within TOMCAT-GLOMAP to a best-estimate of observed global surface mean concentrations (McNorton et al., 2016; Dlugokencky, 2019).

2.2 Radiative transfer model

Radiative effects of O_3 changes are calculated using an O_3 radiative kernel approach, derived using an offline version of the Edwards and Slingo (1996) radiative transfer model. This considers six bands in the shortwave (SW), nine bands in the longwave (LW) and uses a delta-Eddington two-stream scattering solver at all wavelengths (Rap et al., 2015). This version has been used extensively in conjunction with TOMCAT/GLOMAP for calculating radiative forcing from simulated distributions of several short-lived climate pollutants (SLCPs) including BC, O_3 and CH_4 (Spracklen et al., 2011; Riese et al., 2012; Rap et al., 2013; Richards et al., 2013; Rap et al., 2015).

Atmospheric
Chemistry
and Physics
Discussions

2.3 Simulations

All simulations are performed for 1997-2014 with a four-year spin-up through 1993-1996. The control run (CTRL) allows all
150   emissions and meteorology to vary throughout the modelled period. GFED biomass burning emission inventories began in
1997, therefore the 1993-1996 spin-up simulation uses repeating 1999 emissions instead, as the closest year of 'average'
emissions, having excluded 1997 and 1998 due to the exceptionally high emissions in those years (Schultz et al., 2008).

To test the impact of El Niño events on atmospheric chemistry, we performed 4 simulations listed in Table 1. Where model
simulations used "Fixed" parameters in Table 1, the year 2013 emissions or meteorology are specified as invariant throughout
155   the simulation. This year is chosen as the ENSO-neutral case, due to it being the least active ENSO year during 1997-2014,
with a maximum bimonthly multivariate ENSO index (MEI) magnitude of -0.4 and the only year without a single MEI value
that could be considered an active El Niño or La Niña (Wolter and Timlin, 1993; Wolter and Timlin, 1998). We perform
factorial simulations, in which we in turn fix global biomass burning emissions (FIREFIX) and global meteorology (METFIX)
to the 'ENSO-neutral' case. An additional perturbed simulation was performed in order to examine the secondary impact of
160   CO on CH_4 via oxidation changes, where only CO emissions from biomass burning were fixed (COFIX).

Table 1. Details of simulations. All simulations are run for 1997-2014.

Simulation I.D.	Meteorology	CO biomass burning emissions	All other biomass burning emissions
CTRL	Varying	Varying	Varying
METFIX	Fixed	Varying	Varying
FIREFIX	Varying	Fixed	Fixed
COFIX	Varying	Fixed	Varying

3 Model Evaluation

165   We have conducted a comprehensive evaluation of the TOMCAT-GLOMAP coupled model using aircraft observations, and
data from ozone sondes and satellites. In general the model is able to capture absolute concentrations, global distribution and
seasonal variations of major species including O_3, CO and CH_4. MOPITT satellite retrievals have been used to evaluate CO at
800hPa and 500hPa (Emmons et al., 2004) which are shown in Fig. S1 and S2 respectively. TOMCAT performs similarly here
as in Monks et al. (2017), underestimating CO concentrations in the Northern Hemisphere (NH) while overestimating peak
170   concentrations in biomass burning regions, with a maximum difference of ~75ppb (Fig. S1 and S2). However, TOMCAT is
able to reproduce seasonal variations in CO and locates peak CO accurately over East Asia and Central Africa.

TOMCAT was also compared with satellite observations of lower tropospheric (0-6km) O_3 from the Ozone Monitoring
Instrument (OMI). These data were provided by the Rutherford Appleton Laboratory (RAL; data version fv0214) using an
optimal estimation retrieval scheme which resolves O_3 in the 0-6km layer by exploiting information in the Hartley and Huggins
175   uv bands. The scheme derives from that discussed by Miles et al. (2015) for another UV sounder GOME-2. TOMCAT
representation of O_3 concentrations between 0-6 km in NH winter are slightly improved on the Monks et al. (2017) version,
particularly in tropical and Southern Hemisphere (SH) concentrations (Fig. S3). However, there remains a general low bias in
global O_3 of up to 10 Dobson Units (DU) in winter in regions such as the southern Atlantic Ocean.

O_3 has also been evaluated using sonde observations (Fig. S4) (Tilmes et al., 2011), with TOMCAT generally representing
180   the vertical profiles and absolute concentrations of O_3 very well at the majority of sites. There is no apparent regional or
latitudinal bias, although simulated concentrations are significantly over-estimated in India. In addition, the TOMCAT
simulated global tropospheric burden of O_3 in 2000 is 342 Tg which falls within the range of published value (Table 2).

3.1 Aircraft observations

185   We compare annual mean simulated gas-phase species for 1999 against a climatological dataset of aircraft observations from 16 campaigns conducted from 1992 to 2001, with a broad spatial and temporal range (Emmons et al., 2010). Figure 1 shows the comparison of simulated annual mean global concentrations of O_3, CO, CH_4 and NO_x, with aircraft observations at 0- 2 km, 2-6 km and 6-10 km. Full details of the aircraft measurement campaigns used can be found in the Supplementary Table S1.
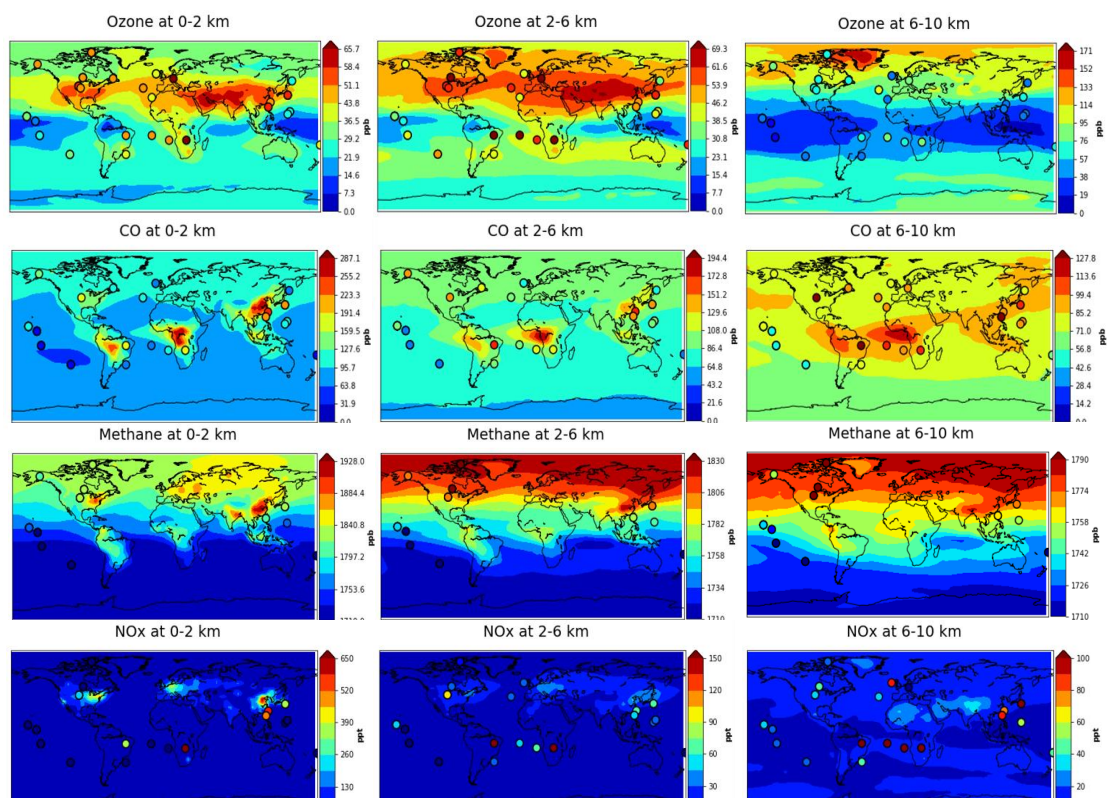

Figure 1: Global annual mean mixing ratios of O_3 (ppb), CO (ppb), CH_4 (ppb) and NO_x (ppt) from TOMCAT at 0-2 km, 2-6 km and 6-10 km. The filled circles show mean values from aircraft observations (Emmons et al., 2010).

190   The model tends to perform better near the surface level for all species, simulating higher concentrations in polluted urban or biomass burning regions, with lower concentrations over ocean and in the SH. O_3 concentrations increase with altitude which is well represented in TOMCAT, although values in the tropics are generally lower than the aircraft observations. CO concentrations decrease with altitude but highest values are still around urban areas and burning regions, which can be seen in both model and aircraft concentrations. Aircraft observations show CH_4 also decreases with altitude and the hemispherical

195   disparity becomes more pronounced, with higher concentrations in the NH. Absolute concentrations in TOMCAT simulations match aircraft data very well and the latitudinal gradient is well captured. At 2-6 km and 6-10 km simulated concentrations are lower than observations at the majority of sites for NO_x. Given NO_x has a short lifetime of less than 1 day (Beirle et al., 2004; Liu et al., 2016), it is difficult for global models, such as TOMCAT, to reproduce observations due to their coarse horizontal and vertical resolutions (Huijnen et al., 2010).

200

Atmospheric
Chemistry
and Physics
Discussions

3.2 OH Evaluation

Due to the very short lifetime of OH, it is challenging to evaluate model simulated OH over representative spatial and temporal scales. Here we follow the evaluation methodology recommended by Lawrence et al. (2001), which was also used to evaluate a previous version of TOMCAT (vn1.76) by Monks et al. (2017). Figure 2 shows our simulated OH compared to Monks et al.

205 (2017), the ACCMIP model mean (Naik et al., 2013) and the Spivakovsky et al. (2000) OH dataset estimated from methyl chloroform observations.

The models and observationally-constrained distribution broadly agree with the latitudinal spread of OH concentrations with a minimum in the SH and a maximum at the tropics; however there is disagreement over the exact altitude of the maximum OH concentrations. In both versions of TOMCAT the highest concentration is between the surface and 750hPa, while ACCMIP

210 and Spivakovsky find peak OH in the upper and mid-level troposphere, respectively. The updated cloud fields used in the current TOMCAT-GLOMAP version have slightly increased OH concentrations in the mid-level and upper domains compared to Monks et al. (2017) but concentrations remain significantly higher in the NH and surface domains than in other studies. In addition, our simulated NH:SH ratio of 1.48 in the current TOMCAT version remains substantially higher than in the ACCMIP models (1.28 ± 0.1), indicating that TOMCAT photolysis rates and OH production in the NH are larger.

215 The total global tropospheric average OH in this version of TOMCAT is 1.04×10^6 molecules cm^{-3}, a decrease from Monks et al. (2017) and within the range of other published values (Table 2). The tropospheric O_3 burden of 342 Tg has increased relative to Monks et al. (2017) (331 Tg) and is within the range found in Wild (2007) (335 ± 10) and ACCMIP models (337 ± 23) (Young et al., 2013). Due to the long lifetime of CH_4, its atmospheric lifetime cannot be determined from TOMCAT simulations. Instead a chemical lifetime is calculated from CH_4 and OH burdens, disregarding stratospheric and soil sinks

220 (Fuglestvedt et al., 1999; Berntsen et al., 2005; Voulgarakis et al., 2013). The lifetime diagnosed from TOMCAT is 8 years, compared to the multi-model mean and range of 9.3 ± 0.9 years from Voulgarakis et al. (2013). The shorter lifetime in TOMCAT is due to the overestimation of OH at the surface, particularly in the NH where CH_4 concentrations are highest due to anthropogenic emissions.
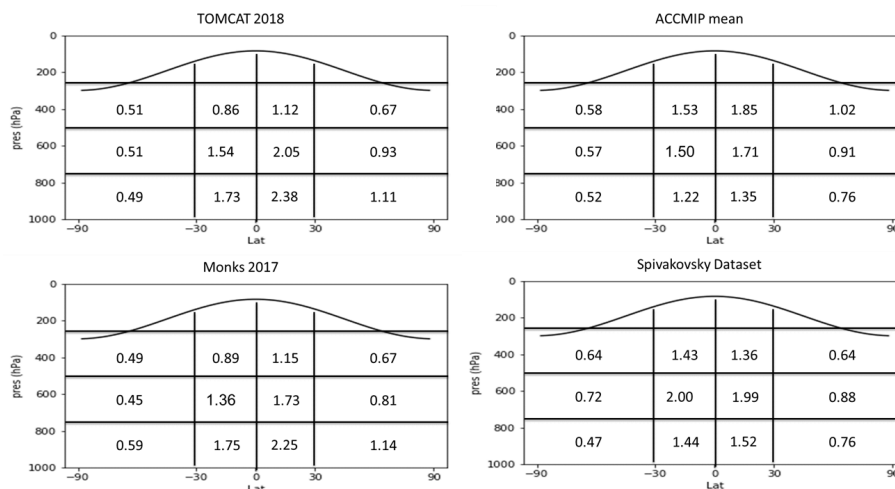

225 **Figure 2: Annual zonal means of hydroxyl radical (OH) concentrations ($\times 10^6$ molecules cm^{-3}) divided into 12 sub-sections as recommended by Lawrence et al. (2001). The simulated OH from this study is compared to a dataset estimated from methyl chloroform observations (Spivakovsky et al., 2000) and the Atmospheric Chemistry and Climate Model Intercomparison Project (ACCMIP) multi-model mean (Naik et al., 2013). A previous version of TOMCAT from Monks et al. (2017) has also been included. A climatological tropopause, indicated by the smooth black line near**
230 **the top of each panel, has been used to remove stratospheric OH.**

Atmospheric
Chemistry
and Physics
Discussions

Table 2: Present day (2000) TOMCAT model diagnostics compared to previous model version from Monks et al., (2017) and other published values.

Diagnostic	TOMCAT (this study)	Monks et al. (2017)	Other estimates	Reference
O_3 burden (Tg)	342	331	337 ± 23	Young et al. (2013)
Tropospheric OH concentration ($\times 10^6$ molecules cm^{-3})	1.04	1.08	0.94-1.06	Prinn et al. (2001); Krol and Lelieveld (2003); Bousquet et al. (2005); Wang et al. (2008).
CH_4 lifetime (years)	8.0	7.9	9.3 ± 0.9	Voulgarakis et al. (2013)

235

4 Results and discussion

4.1 Impact of meteorology and fire emissions on trace gas interannual variability

First we examine the mechanisms controlling interannual variability of simulated tropospheric CO, O_3 and mean OH. We use the difference between the control simulation (CTRL) and the perturbed simulations with fixed fires (FIREFIX) and fixed

240   meteorology (METFIX) to determine the driving cause of IAV. Of particular interest is the effect of the 1997-1998 El Niño event (henceforth referred to as 1997 El Niño) and how the prevailing mechanisms controlling IAV change during such events. To define El Niño events, we use the bimonthly multivariate ENSO index, which is calculated from 6 observed variables and standardised to accurately monitor ENSO occurrence (Wolter and Timlin, 1998; Wolter and Timlin, 2011).

Previous studies examining the dominant factor controlling global CO IAV have found contrasting results. Szopa et al. (2007)

245   suggested that meteorology was the main driver, accounting for 50-90% of IAV in the tropics. In contrast, Voulgarakis et al. (2015) suggested that biomass burning was the much more dominant driver with only a small effect from meteorology. This assertion is further supported by the study of Monks et al. (2012) of CO IAV in the Arctic, where biomass was found to be dominant. Some of the differences in results can be explained by Szopa et al. (2007) considering only surface CO rather than the whole troposphere as in Voulgarakis et al. (2015). Here we also consider whole tropospheric CO and our results are in line

250   with those from Voulgarakis et al. (2015). We find the dominant source of IAV across the entire period is emissions from biomass burning - indicated by the large difference between simulations CTRL and FIREFIX (Fig. 3a), with a small effect from meteorological changes (CTRL – METFIX). This effect is largest during the 1997 El Niño where an increase in fire events increased CO concentrations by more than 40%. Smaller increases occur in 2002/2003 and 2006 during less extreme El Niño events, but the effect is not seen during the 2009/2010 El Niño, indicating that El Niño only significantly impacts CO

255   concentrations when there is an associated increase in global fire events.

Expanding on the work of Voulgarakis et al. (2015), we analysed IAV using a coefficient of variation (CV), calculated as the multi-year standard deviation normalised by the mean (Fig. 4). The global annual mean CO IAV over the whole period is 11.0% for the whole troposphere, 14.3% for surface concentrations. This is in very good agreement with Voulgarakis et al. (2015) who calculated 10% IAV, and even better when we consider the same time period (2005-2009) when IAV decreases

260   to 9.7%. However, there are regional differences; CO IAV from TOMCAT is much larger in high-latitude boreal regions. This is due to the difference in period studied meaning this study includes additional extreme events including unusually large Russia boreal wildfires in 2010 and 2012 (Gorchakov et al., 2014; Kozlov et al., 2014). Infrequent and extreme events such as these significantly increase IAV.

Atmospheric
Chemistry
and Physics
Discussions

CO IAV is significantly greater in September-October, with peaks in known fire regions such as tropical South America,

265   Africa, Southeast Asia and in boreal forests. This indicates a strong contribution of fire emissions to IAV especially from Indonesia, as also suggested by the analysis of Fig. 3a and previous studies (Monks et al., 2012; Huang et al., 2014; Voulgarakis et al., 2015). In the FIREFIX simulation IAV is ~55% of the CTRL value showing a large reduction in variability when interannual variability in fire emissions is removed. The IAV in March-April is significantly smaller than September-October as this period is outside the primary fire season for South America and Eurasia, although hotspots remain in Southeast Asia

270   and Africa where fires commonly occur in March-April (van der Werf et al., 2017). Meteorology and atmospheric transport changes are most important in Africa in September-October and Indonesia in March-April (Fig. 4c, d). Fire emissions occur in these regions but the meteorological effects are important sources of IAV. This is in good agreement with Voulgarakis et al. (2015) who found that with fixed biomass burning emissions there remained high IAV over Africa during Dec-Jan, and Huang et al. (2014) who found CO over Central Africa correlated more closely with ice water content than CO emissions.

275   However, the overall effect of meteorology on global IAV found here is much smaller than the 50-90% suggested by Szopa et al. (2007): when we consider only surface CO over the same period, fixing meteorology decreases the mean CO IAV by just 5%.
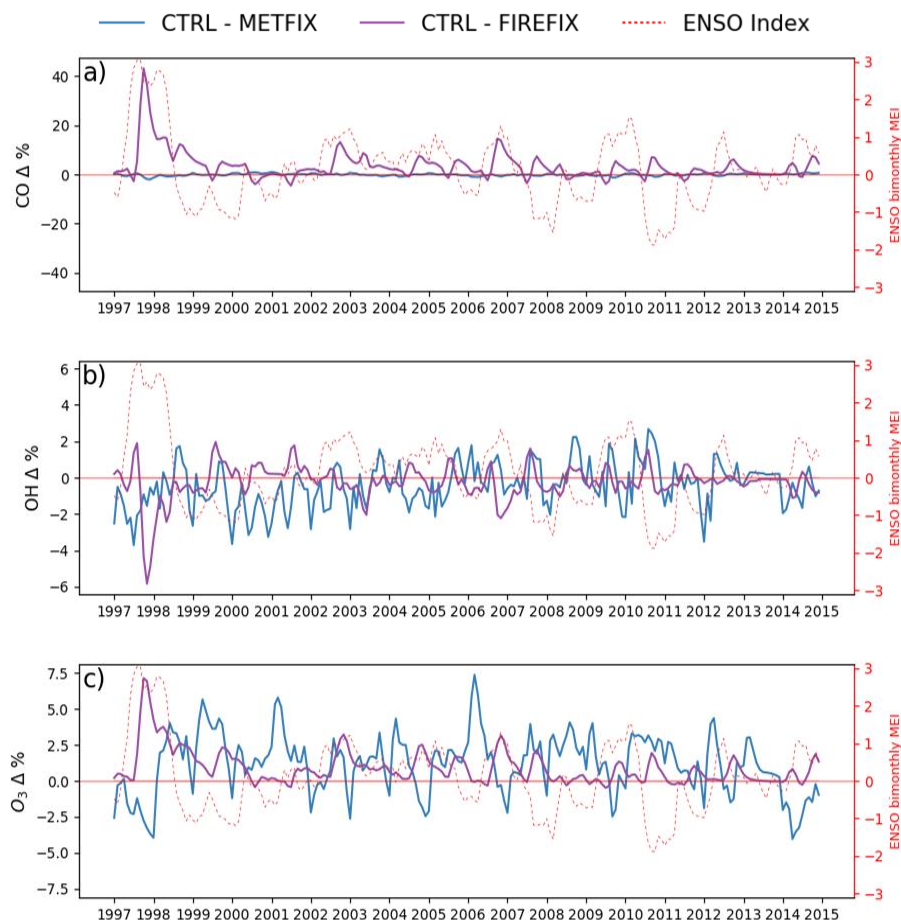
Figure 3: Time series of simulated differences (%) between the control and the fixed meteorology (CTRL - METFIX, blue line) and fixed fire emissions (CTRL – FIREFIX, purple line) simulations for the global tropospheric burden of (a) CO, (b) OH and (c) O₃. The ENSO bimonthly mean multivariate index is plotted in the dashed red line on the right-hand y-axis in each panel.
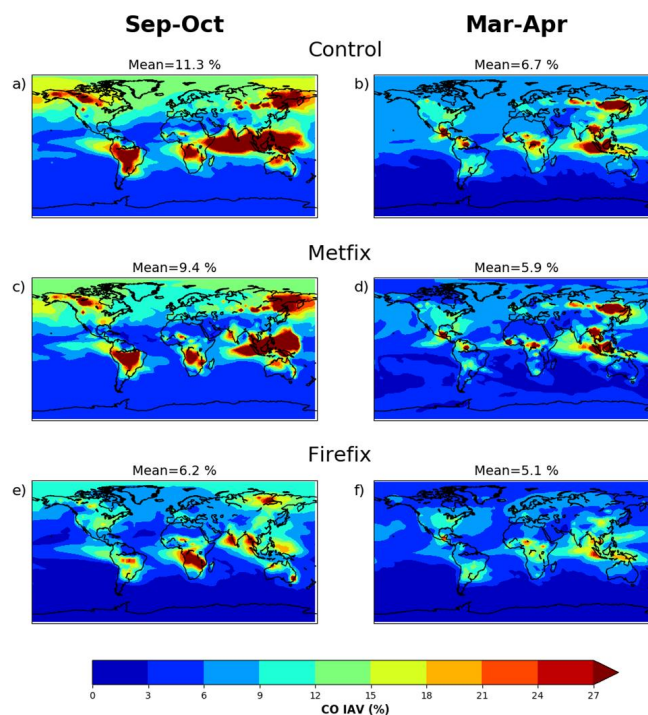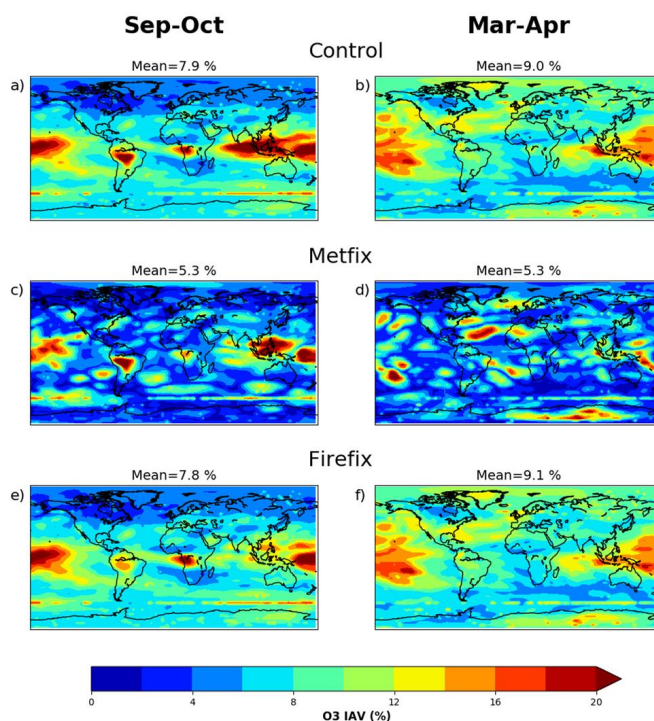
Figure 4: The interannual variability (coefficient of variation) of CO over the period 1997-2014. Calculated for September – October (left panels) and March - April (right panels) for (a, b) control simulation (CTRL), (c, d) fixed meteorology (METFIX) and (e, f) fixed fire emissions (FIREFIX).

The IAV of OH and O_3 have more complex contributions from fire emissions and meteorology (Fig. 3b, c). For both species

280   meteorology is the dominant cause of variability for the majority of the period, indicated by on-average greater deviation from CTRL in METFIX simulation than FIREFIX, including during El Niño events outside of the 1997 El Niño, such as in 2006. However, fire emissions are the dominant cause of variation during the 1997 El Niño for both species, increasing tropospheric O_3 burden by ~7% and decreasing tropospheric OH by ~6%. This indicates that while meteorology is the most important driver of IAV in global OH and tropospheric O_3, fire emissions also play a key role, sometimes even becoming the dominant driver

285   when there are particularly large fire emissions during El Niño conditions.

Figure 5 shows the IAV of O_3, supporting the analysis of Fig. 4 that also suggests meteorology is the dominant process in controlling IAV. METFIX-simulated IAV differs substantially from the CTRL, with much lower IAV in Sept-Oct (33% decrease) and in Mar-Apr (42% decrease) when meteorology is repeated. However, in the METFIX run there remain peaks in variability in close proximity to regions with large biomass burning emissions, demonstrating the significant contribution from fire emissions. In the FIREFIX simulation the distribution of IAV is broadly similar to the CTRL simulation and with only a small change in global mean CV, indicating that fire emissions have less control on O_3 IAV. These results are again comparable to Voulgarakis et al. (2015) as the distribution of O_3 IAV in both CTRL and FIREFIX simulations is similar although with slightly larger values of variation due to differing time period.

Figure 5: The interannual variability (coefficient of variation) of ozone over the period 1997-2014. Calculated for September – October (left panels) and March - April (right panels) for (a, b) control simulation (CTRL), (c, d) fixed meteorology (METFIX) and (e, f) fixed fire emissions (FIREFIX).

4.2 Indirect effect of CO on oxidation and lifetime of CH_4

The COFIX sensitivity experiment was conducted to determine the indirect influence of CO emissions on CH_4 variability through changes in tropospheric OH concentrations. Figure 6a shows the difference in COFIX monthly mean OH concentrations from the control experiment, compared to that from the METFIX and FIREFIX simulations. Over the whole period, the inclusion of CO emissions from biomass burning consistently decreases tropospheric OH concentrations. This is due to the reaction of CO with OH which is the primary sink of CO. The greatest impact is during the 1997 El Niño where CO emissions were abnormally large, suppressing mass weighted global mean OH concentrations by up to 9%. This effect on OH in TOMCAT is considerably larger than that simulated by Butler et al. (2005), who also found an increase in CO during the 1997 El Niño and subsequent decrease OH of 2.2%. The suppression of OH concentrations due to CO emission is also simulated to a lesser degree in the 2003 and 2006 El Niño events, but is absent in 2010 El Niño as this event had little impact

Atmospheric
Chemistry
and Physics
Discussions

on global fire occurrence (Randerson et al., 2017). The effect of fixing only CO from fires is greater than the effect of fixing

305   all fire emissions due to co-emitted species such as NO_x, which act to increase OH concentrations.
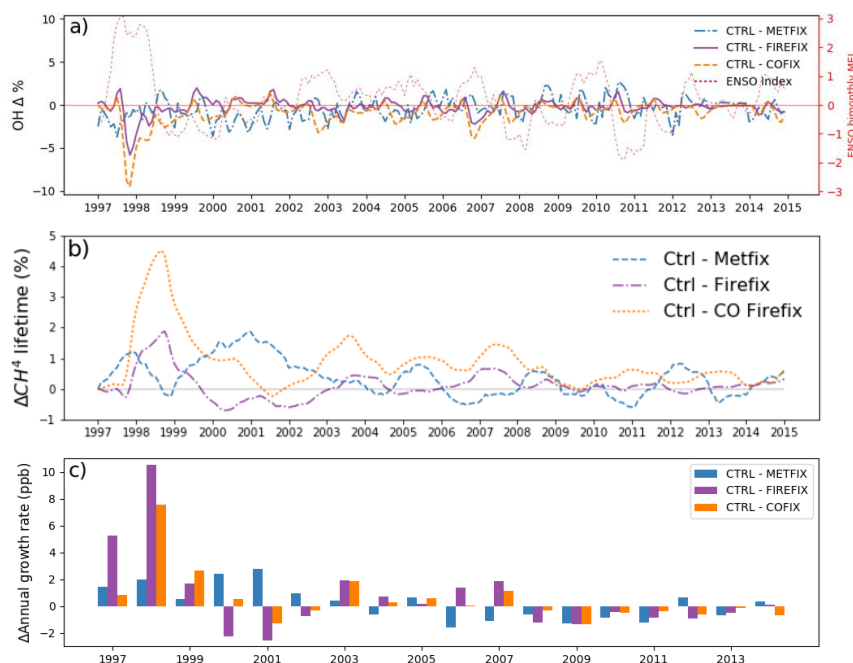
Figure 6: Time series of (a) the change in mass-weighted tropospheric OH (%), (b) change in CH_4 lifetime (%) and (c) resultant change in annual growth rate calculated using an offline box model. The ENSO bimonthly mean multivariate index is plotted in the dashed red line on the right-hand y-axis in panel (a).

As OH is also the primary sink of CH_4 (~90%) (McNorton et al., 2016), another effect of the decrease in OH due to CO emissions is to weaken the sink of CH_4, increasing its atmospheric lifetime. The magnitude of this can be seen in Fig. 6b; the

310   COFIX simulation indicates that CO emissions from fires extend CH_4 atmospheric lifetime by more than 4% during the 1997 El Niño. Fixing all fire emissions also enhances CH_4 lifetime by around 2%. Increasing the lifetime of a species increases its concentration in steady-state equilibrium. Due to the scaling applied to CH_4 in TOMCAT we are unable to directly calculate the response in CH_4 growth rate from TOMCAT, as simulated CH4 concentrations are nudged to the observed global mean surface value. Therefore, to determine the impact of the change to OH on CH_4 concentrations we used a simple global box

315   model. This box model is similar to that described in McNorton et al. (2016), which was found to compare well with other global and 12-box CH_4 models (Rigby et al., 2013; McNorton et al., 2016). In this case, the box model used monthly mean tropospheric OH concentrations and CH_4 emissions for each simulation while assuming constant temperature to calculate the effect of changing OH on global mean surface CH_4. The impact of fire emissions on the CH_4 growth rate is greatest in 1998, where all emissions from fires increased global CH_4 by 10.5 ppb (Fig. 6c). Analysis of the COFIX simulation demonstrates

320   that up to 7.5 ppb (72%) of that change could have been caused by the release of CO alone and its role as a sink for OH. The effect on growth rate in the FIREFIX simulation is larger than the COFIX despite a greater effect on CH_4 lifetime from the COFIX, due to directly emitted CH_4 varying with El Niño conditions in the COFIX simulation and not in FIREFIX. The influence of CO emissions on CH_4 growth rate calculated here is smaller than in Butler et al. (2005) despite a much larger effect on tropospheric OH. The radiative effect of the change to CH_4 from CO emitted from biomass burning alone in 1998 is

325   0.004 Wm^{-2}, calculated using updated expressions from Etminan et al. (2016).

4.3 Limiting factors of O₃ production

The ratio between formaldehyde (HCHO) and nitrogen dioxide (NO$_2$) concentrations can be used to indicate the limiting factor for tropospheric O$_3$ production (Duncan et al., 2010). Ratios smaller than 1 indicate that removing VOCs will decrease tropospheric O$_3$ formation (i.e. a VOC-limited regime), while ratios larger than 2 indicate that removing NO$_x$ will reduce O$_3$

330   (i.e. a NO$_x$-limited regime). Ratios of 1-2 indicate that both NO$_x$ and VOC reductions could decrease O$_3$ (i.e. a 'both-limited' regime). Here we apply this methodology to determine the changes to this ratio from 1997-2014 and dependence of O$_3$ formation during the 1997 El Niño event. We compare the early period mean (1997-2001) to the end period mean (2010-2014) to determine whether significant changes have occurred over the 18-year period, and compared mean El Niño conditions to both.

335   In general, the SH and tropical regions have a very high ratios, meaning they are strongly NO$_x$-limited (Fig. 7). The NH is also predominantly NO$_x$-limited although less robustly and polluted regions tend to be either VOC-limited or both-limited regimes. The ratio is largely constant across the modelled period, however there are some significant shifts such as in India, which was once solely NO$_x$-limited, becoming increasing VOC-limited due to increased NO$_x$ pollution (Hilboll et al., 2017).

During El Niño there are large changes; increasing the ratio and therefore NO$_x$ limitation by more than 40% in the Tropical

340   Pacific. Significant changes to the ratio were also found in biomass burning regions of South America and Southeast Asia. This is due to the increase in NO$_x$ emissions in larger fire seasons associated with El Niño. However, these regions are already very heavily NO$_x$-limited due to high VOC emissions in forest regions, meaning that although the shift in HCHO/NO$_2$ ratio during El Niño is large, it is not substantial enough to alter the limiting factor for formation of tropospheric O$_3$ from one regime to another. Over India, El Niño causes the solely NO$_x$-limited regime from the beginning of the period to persist throughout.

345
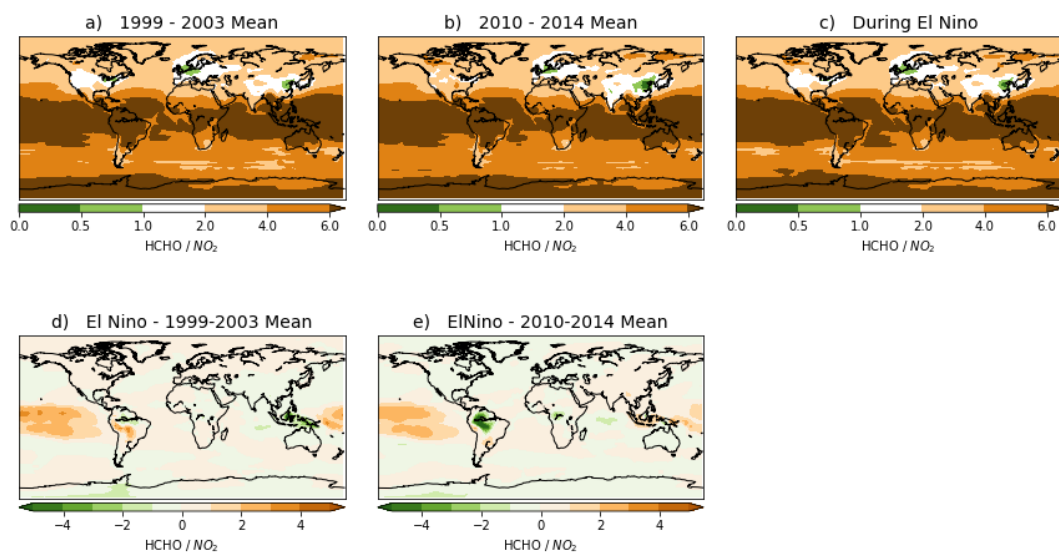
Figure 7: 5-year mean of the ratio of tropospheric column HCHO to NO₂ at (a) the beginning of model period (1999-2003), (b) end of model period (2010-2014) and (c) mean ratio value during all El Niño events. Panels (d) and (e) show difference during El Niño from the 5-year mean values in panels (a) and (b), respectively.

4.4 Impact on tropospheric ozone and radiative effects

The 1997 El Niño significantly altered the vertical distribution of O_3 in the troposphere – increasing O_3 concentrations in the NH while decreasing in the SH and tropics with an overall decrease in tropospheric O_3 of -0.82% compared to the 1997-2014 mean (Fig. 8a). There are also very large increases in the mid-latitude upper troposphere of both hemispheres in the CTRL and

350　FIREFIX simulations but not in METFIX, implying that this is produced by El Niño-associated meteorological processes which promote intrusion of stratospheric air into the troposphere. In general the METFIX run simulates much higher O_3 concentrations in the NH than the period mean and lower concentrations in the SH (Fig. 8b). There is an overall increase in O_3 (~2%) when meteorology was fixed to an ENSO-neutral year (i.e. 2013), meaning that meteorology during the 1997 El Niño caused a decrease in tropospheric O_3 concentrations despite large increases in O_3 in regions of the upper troposphere due to

355　stratospheric intrusion. In the 1997 El Niño we find a 0.4% increase in global tropospheric humidity compared to the period mean. This is likely responsible for the decrease in O_3 due to meteorology as increased humidity enhances O_3 loss (Stevenson et al., 2000; Isaksen et al., 2009; Kawase et al., 2011). Changes to transport and distribution of O_3 will also impact how effectively tropospheric O_3 is produced and lost.

The similarities between the tropospheric O_3 distribution in the CTRL and FIREFIX simulations shows that fire emissions

360　have a relatively small impact on the global distribution of O_3, but do affect absolute values, as concentrations in the FIREFIX run are significantly lower at the tropics. This is likely because of the removal of large emissions of O_3 precursors in that latitude band when fire emissions are fixed to a non-El Niño year.
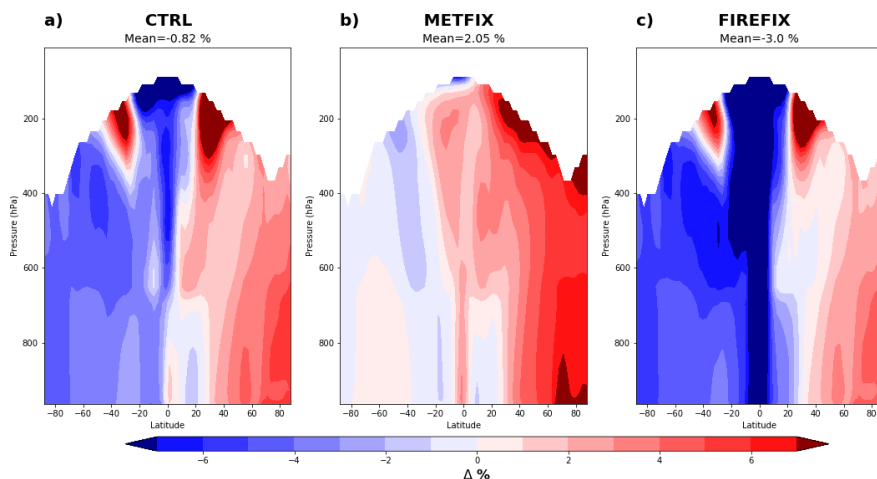

Figure 8: Latitude-pressure profiles of the percentage difference in O_3 concentration during 1997 El Niño event compared to 1997-2014 period mean for simulations (a) CTRL, (b) METFIX and (c) FIREFIX.

Figure 9 shows the tropospheric O_3 radiative effect (RE) during the 1997 El Niño in each TOMCAT simulation, calculated

365　using the Rap et al. (2015) tropospheric O_3 radiative kernel. Consistent with the relative changes in O_3 concentration, fire emissions and meteorology have contrasting effects on O_3 RE. When isolated, these effects are opposite and almost equal: fire emissions increase O_3 RE by 0.031 Wm^{-2} while meteorology decreases by -0.030 Wm^{-2}. We performed an additional simulation to determine the effect of these factors occurring simultaneously (BOTHFIX) - and found the increasing effect from fire emissions to be dominant over the decreasing effect from meteorology, leading to an overall increase in global mean O_3 RE

370　of 0.015 $W m^{-2}$.

The effect of fire emissions occurs almost entirely over Indonesia and the Eastern Indian Ocean where the large influx of NO_x, CO, CH_4 and other O_3 precursors from fire emissions during the 1997 El Niño causes regional increases in tropospheric O_3 RE of up to 0.17 Wm^{-2}. Meteorology has more varied impacts during El Niño; causing large decreases in O_3 RE over the Central

375   Pacific Ocean (~ -0.36 Wm^{-2}) but also increases in the mid-latitudes of the Pacific Ocean (~0.33 Wm^{-2}). Globally the mean change to O_3 RE is small, around 0.015 Wm^{-2}, but large regional changes have the potential to significantly alter atmospheric heating and dynamics.
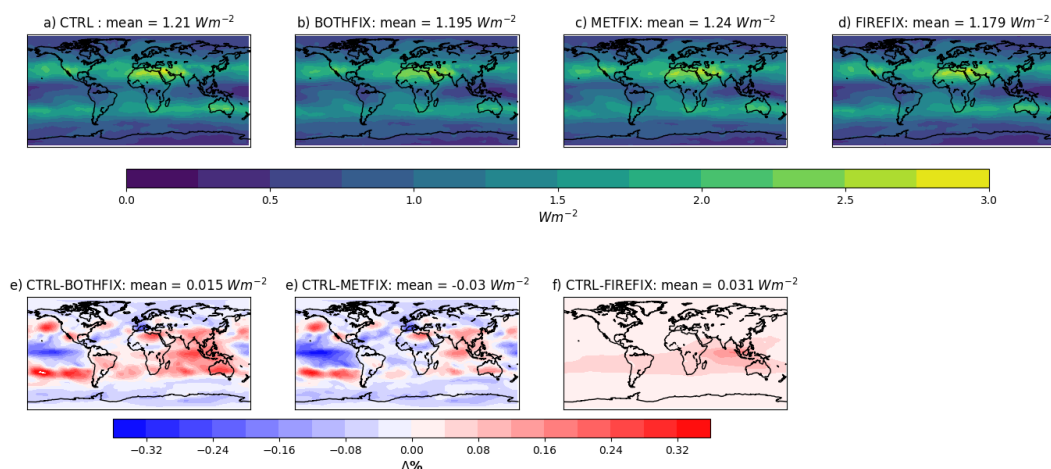
Figure 9: Tropospheric O_3 radiative effects (Wm^{-2}) from the TOMCAT simulations (a) control, (b) fixed meteorology and fixed fire emissions, (c) fixed meteorology only and (d) fixed fire emissions only (d). Panels (e-g) show percentage differences between the control and the three perturbed simulations.

6 Summary and conclusions

Global model simulations using annually invariant meteorology and fire emissions were performed for the period 1997-2014
380   in order to determine their relative impacts on IAV of O_3 and CH_4, particularly during El Nino events. The TOMCAT-GLOMAP model used has been updated compared to that described by Monks et al. (2017) with improved cloud and photolysis representation and the introduction of Martensson sea spray emissions (Gordon et al., 2017). Model simulations were evaluated for a number of chemical species (O_3, CH_4, NO_x, CO) with observations from aircraft, satellites and ozone sondes. In general, the model shows a reasonable agreement with observed values although there are some regional and seasonal biases.
385   Differences between model and observations may be due to numbers of factors such as the relatively coarse model resolution, uncertainties in the model emission inventories and errors in observations. However, good overall agreement of model simulations with multiple observations gives us the confidence in model performance to support the results.

The IAV of global CO concentrations is large and are primarily controlled by fire emissions over the modelled period. Exceptionally large CO emissions linked to El Niño in 1997 led to a decrease in OH concentrations of ~9%, which subsequently
390   increased CH_4 lifetime by ~4%. Using a box model we quantify the isolated impact of this change in atmospheric chemistry on global CH_4 growth rate to be 7.75 ppb, ~75% of the total effect of fires. This effect, combined with concurrent direct CH_4 emission from fires explains the observed changes to CH_4 growth rate during the 1997 El Niño.

Variability of oxidants O_3 and OH is far more dependent on meteorology than fire emissions, except during very large El Niño
395   events such as in 1997 and 1998, when fires become dominant in terms of total tropospheric burden although meteorology still

controls distribution. The change to tropospheric O_3 concentrations during El Niño has increased O_3 RF by 0.17 Wm^{-2} over Southeast Asia and decreased by 0.36 Wm^{-2} over the Central Pacific. The global mean O_3 RF change due to 1997 El Niño meteorology and fires is an increase of 0.015 Wm^{-2}, as emissions of O_3 precursors from fires causes increased O_3. El Niño also causes significant shifts in the ratio of $HCHO/NO_x$ – an indicator of O_3 production regime – but most significantly in the tropics which are heavily NO_x-limited, so this change does not cause a regime shift.

We have shown that El Niño events significantly affect the variability of two important drivers of anthropogenic climate change. Further research into how El Niño events, and their effect on fire emissions, is likely to change in a warming climate is required to understand how these links between ENSO and CH_4 and O_3 may change and influence future climate change mitigation attempts.

Author contribution

MR, AR and SA conceptualised the study and planned the experiments. MC, KP, HG, WF and MR developed and evaluated the version of TOMCAT-GLOMAP used here. BK, BL and RS provided the satellite retrievals for the O_3 comparison which was conducted by RP. MC and JM provided assistance and advice for the CH_4 box model. MR performed the TOMCAT model runs, SOCRATES and box model calculations. MR analysed the results with help from AP and SA. MR compiled results and prepared the manuscript. All co-authors contributed to the final version with comments.

Acknowledgements

Atmospheric
Chemistry
and Physics
Discussions

Open Access

References

Anenberg, S. C., Horowitz, L. W., Tong, D. Q., and West, J. J.: An Estimate of the Global Burden of Anthropogenic Ozone and Fine Particulate Matter on Premature Human Mortality Using Atmospheric Modeling, Environmental Health Perspectives, 118, 1189-1195, doi:10.1289/ehp.0901220, 2010.

420 Beirle, S., Platt, U., von Glasow, R., Wenig, M., and Wagner, T.: Estimate of nitrogen oxide emissions from shipping by satellite remote sensing, Geophysical Research Letters, 31, doi:10.1029/2004GL020312, 2004.

Berntsen, T. K., Fuglestvedt, J. S., Joshi, M. M., Shine, K. P., Stuber, N., Ponater, M., Sausen, R., Hauglustaine, D. A., and Li, L.: Response of climate to regional emissions of ozone precursors: sensitivities and warming potentials, Tellus B: Chemical and Physical Meteorology, 57, 283-304, 10.3402/tellusb.v57i4.16549, 2005.

425 Bousquet, P., Hauglustaine, D. A., Peylin, P., Carouge, C., and Ciais, P.: Two decades of OH variability as inferred by an inversion of atmospheric transport and chemistry of methyl chloroform, Atmos. Chem. Phys., 5, 2635-2656, 10.5194/acp-5-2635-2005, 2005.

Bousquet, P., Ciais, P., Miller, J. B., Dlugokencky, E. J., Hauglustaine, D. A., Prigent, C., Van der Werf, G. R., Peylin, P., Brunke, E. G., Carouge, C., Langenfelds, R. L., Lathière, J., Papa, F., Ramonet, M., Schmidt, M., Steele, L. P., Tyler, S. C., and
430 White, J.: Contribution of anthropogenic and natural sources to atmospheric methane variability, Nature, 443, 439, 10.1038/nature05132
https://www.nature.com/articles/nature05132#supplementary-information, 2006.

Butler, T. M., Rayner, P. J., Simmonds, I., and Lawrence, M. G.: Simultaneous mass balance inverse modeling of methane and carbon monoxide, Journal of Geophysical Research: Atmospheres, 110, doi:10.1029/2005JD006071, 2005.

435 Chen, Y.-H., and Prinn, R. G.: Estimation of atmospheric methane emissions between 1996 and 2001 using a three-dimensional global chemical transport model, Journal of Geophysical Research: Atmospheres, 111, doi:10.1029/2005JD006058, 2006.

Chipperfield, M. P.: New version of the TOMCAT/SLIMCAT off-line chemical transport model: Intercomparison of stratospheric tracer experiments, Quarterly Journal of the Royal Meteorological Society, 132, 1179-1203,
440 doi:10.1256/qj.05.51, 2006.

Corbett, A., Jiang, X., Xiong, X., Kao, A., and Li, L.: Modulation of midtropospheric methane by El Niño, Earth and Space Science, 4, 590-596, doi:10.1002/2017EA000281, 2017.

Dlugokencky, E.: NOAA/ESRL, (www.esrl.noaa.gov/gmd/ccgg/trends_ch4/), 2019.

Dlugokencky, E. J., Nisbet, E. G., Fisher, R., and Lowry, D.: Global atmospheric methane: budget, changes and dangers,
445 Philosophical Transactions of the Royal Society A: Mathematical, Physical and Engineering Sciences, 369, 2058-2072, 10.1098/rsta.2010.0341, 2011.

Duncan, B., Yoshida, Y., R. Olson, J., Sillman, S., Martin, R., Lamsal, L., Hu, Y., E. Pickering, K., Retscher, C., and J. Allen, D.: Application of OMI observations to a space-based indicator of NOx and VOC controls on surface ozone formation, 2213-2223 pp., 2010.

450 Emmons, L. K., Deeter, M. N., Gille, J. C., Edwards, D. P., Attié, J.-L., Warner, J., Ziskin, D., Francis, G., Khattatov, B., Yudin, V., Lamarque, J.-F., Ho, S.-P., Mao, D., Chen, J. S., Drummond, J., Novelli, P., Sachse, G., Coffey, M. T., Hannigan, J. W., Gerbig, C., Kawakami, S., Kondo, Y., Takegawa, N., Schlager, H., Baehr, J., and Ziereis, H.: Validation of Measurements of Pollution in the Troposphere (MOPITT) CO retrievals with aircraft in situ profiles, Journal of Geophysical Research: Atmospheres, 109, doi:10.1029/2003JD004101, 2004.

455 Emmons, L. K., Walters, S., Hess, P. G., Lamarque, J.-F., Pfister, G. G., Fillmore, D., Granier, C., Guenther, A., Kinnison, D., Laepple, T., Orlando, J., Tie, X., Tyndall, G., Wiedinmyer, C., Baughcum, S. L., and Kloster, S.: Description and evaluation of the Model for Ozone and Related chemical Tracers, version 4 (MOZART-4), Geoscientific Model Development, 3, 43-67, 10.5194/gmd-3-43-2010, 2010.

Etminan, M., Myhre, G., Highwood, E. J., and Shine, K. P.: Radiative forcing of carbon dioxide, methane, and nitrous oxide: A
460 significant revision of the methane radiative forcing, Geophysical Research Letters, 43, 12,614-612,623, doi:10.1002/2016GL071930, 2016.

Feely, R. A., Gammon, R. H., Taft, B. A., Pullen, P. E., Waterman, L. S., Conway, T. J., Gendron, J. F., and Wisegarver, D. P.: Distribution of chemical tracers in the eastern equatorial Pacific during and after the 1982–1983 El Niño/Southern Oscillation event, Journal of Geophysical Research: Oceans, 92, 6545-6558, doi:10.1029/JC092iC06p06545, 1987.

465 Fuglestvedt, J. S., Berntsen, T. K., Isaksen, I. S. A., Mao, H., Liang, X.-Z., and Wang, W.-C.: Climatic forcing of nitrogen oxides through changes in tropospheric ozone and methane; global 3D model studies, Atmospheric Environment, 33, 961-977, https://doi.org/10.1016/S1352-2310(98)00217-9, 1999.

Gorchakov, G. I., Sitnov, S. A., Sviridenkov, M. A., Semoutnikova, E. G., Emilenko, A. S., Isakov, A. A., Kopeikin, V. M., Karpov, A. V., Gorchakova, I. A., Verichev, K. S., Kurbatov, G. A., and Ponomareva, T. Y.: Satellite and ground-based
470 monitoring of smoke in the atmosphere during the summer wildfires in European Russia in 2010 and Siberia in 2012, International Journal of Remote Sensing, 35, 5698-5721, 10.1080/01431161.2014.945008, 2014.

Gordon, H., Kirkby, J., Baltensperger, U., Bianchi, F., Breitenlechner, M., Curtius, J., Dias, A., Dommen, J., Donahue, N. M., Dunne, E. M., Duplissy, J., Ehrhart, S., Flagan, R. C., Frege, C., Fuchs, C., Hansel, A., Hoyle, C. R., Kulmala, M., Kürten, A., Lehtipalo, K., Makhmutov, V., Molteni, U., Rissanen, M. P., Stozhkov, Y., Tröstl, J., Tsagkogeorgas, G., Wagner, R.,

Atmospheric
Chemistry
and Physics
Discussions

475   Williamson, C., Wimmer, D., Winkler, P. M., Yan, C., and Carslaw, K. S.: Causes and importance of new particle
       formation in the present-day and preindustrial atmospheres, Journal of Geophysical Research: Atmospheres, 122,
       8739-8760, doi:10.1002/2017JD026844, 2017.
       Granier, C., Müller, J.-F., and Brasseur, G.: The Impact of Biomass Burning on the Global Budget of Ozone and Ozone
       Precursors., in: Biomass Burning and Its Inter-Relationships with the Climate System, edited by: Innes J.L., B. M.,
480   Verstraete M.M., Springer, Dordrecht, 2000.
       Hilboll, A., Richter, A., and Burrows, J. P.: NO2 pollution over India observed from space — the impact of rapid economic
       growth, and a recent decline, Atmos. Chem. Phys. Discuss., 2017, 1-18, 10.5194/acp-2017-101, 2017.
       Hodson, E. L., Poulter, B., Zimmermann, N. E., Prigent, C., and Kaplan, J. O.: The El Niño–Southern Oscillation and wetland
       methane interannual variability, Geophysical Research Letters, 38, doi:10.1029/2011GL046861, 2011.
485   Holtslag, A. A. M., and Boville, B. A.: Local Versus Nonlocal Boundary-Layer Diffusion in a Global Climate Model, Journal of
       Climate, 6, 1825-1842, 10.1175/1520-0442(1993)006<1825:Lvnbld>2.0.Co;2, 1993.
       Huang, L., Fu, R., and Jiang, J. H.: Impacts of fire emissions and transport pathways on the interannual variation of CO in the
       tropical upper troposphere, Atmos. Chem. Phys., 14, 4087-4099, 10.5194/acp-14-4087-2014, 2014.
       Huijnen, V., Eskes, H. J., Poupkou, A., Elbern, H., Boersma, K. F., Foret, G., Sofiev, M., Valdebenito, A., Flemming, J., Stein, O.,
490   Gross, A., Robertson, L., D'Isidoro, M., Kioutsioukis, I., Friese, E., Amstrup, B., Bergstrom, R., Strunk, A., Vira, J.,
       Zyryanov, D., Maurizi, A., Melas, D., Peuch, V. H., and Zerefos, C.: Comparison of OMI NO$_2$ tropospheric
       columns with an ensemble of global and European regional air quality models, Atmos. Chem. Phys., 10, 3273-3296,
       10.5194/acp-10-3273-2010, 2010.
       Isaksen, I. S. A., Granier, C., Myhre, G., Berntsen, T. K., Dalsøren, S. B., Gauss, M., Klimont, Z., Benestad, R., Bousquet, P.,
495   Collins, W., Cox, T., Eyring, V., Fowler, D., Fuzzi, S., Jöckel, P., Laj, P., Lohmann, U., Maione, M., Monks, P., Prevot, A.
       S. H., Raes, F., Richter, A., Rognerud, B., Schulz, M., Shindell, D., Stevenson, D. S., Storelvmo, T., Wang, W. C., van
       Weele, M., Wild, M., and Wuebbles, D.: Atmospheric composition change: Climate–Chemistry interactions,
       Atmospheric Environment, 43, 5138-5192, https://doi.org/10.1016/j.atmosenv.2009.08.003, 2009.
       Jones, C. D., Collins, M., Cox, P. M., and Spall, S. A.: The Carbon Cycle Response to ENSO: A Coupled Climate–Carbon Cycle
500   Model Study, Journal of Climate, 14, 4113-4129, 10.1175/1520-0442(2001)014<4113:tccrte>2.0.co;2, 2001.
       Kawase, H., Nagashima, T., Sudo, K., and Nozawa, T.: Future changes in tropospheric ozone under Representative
       Concentration Pathways (RCPs), 38, doi:10.1029/2010GL046402, 2011.
       Kirschke, S., Bousquet, P., Ciais, P., Saunois, M., Canadell, J. G., Dlugokencky, E. J., Bergamaschi, P., Bergmann, D., Blake, D.
       R., Bruhwiler, L., Cameron-Smith, P., Castaldi, S., Chevallier, F., Feng, L., Fraser, A., Heimann, M., Hodson, E. L.,
505   Houweling, S., Josse, B., Fraser, P. J., Krummel, P. B., Lamarque, J.-F., Langenfelds, R. L., Le Quéré, C., Naik, V.,
       O'Doherty, S., Palmer, P. I., Pison, I., Plummer, D., Poulter, B., Prinn, R. G., Rigby, M., Ringeval, B., Santini, M.,
       Schmidt, M., Shindell, D. T., Simpson, I. J., Spahni, R., Steele, L. P., Strode, S. A., Sudo, K., Szopa, S., van der Werf, G.
       R., Voulgarakis, A., van Weele, M., Weiss, R. F., Williams, J. E., and Zeng, G.: Three decades of global methane sources
       and sinks, Nature Geoscience, 6, 813, 10.1038/ngeo1955
510   https://www.nature.com/articles/ngeo1955#supplementary-information, 2013.
       Kozlov, V. S., Yausheva, E. P., Terpugova, S. A., Panchenko, M. V., Chernov, D. G., and Shmargunov, V. P.: Optical–
       microphysical properties of smoke haze from Siberian forest fires in summer 2012, International Journal of Remote
       Sensing, 35, 5722-5741, 10.1080/01431161.2014.945010, 2014.
       Krol, M., and Lelieveld, J.: Can the variability in tropospheric OH be deduced from measurements of 1,1,1-trichloroethane
515   (methyl chloroform)?, Journal of Geophysical Research: Atmospheres, 108, doi:10.1029/2002JD002423, 2003.
       Lamarque, J. F., Bond, T. C., Eyring, V., Granier, C., Heil, A., Klimont, Z., Lee, D., Liousse, C., Mieville, A., Owen, B., Schultz, M.
       G., Shindell, D., Smith, S. J., Stehfest, E., Van Aardenne, J., Cooper, O. R., Kainuma, M., Mahowald, N., McConnell, J.
       R., Naik, V., Riahi, K., and van Vuuren, D. P.: Historical (1850–2000) gridded anthropogenic and biomass burning
       emissions of reactive gases and aerosols: methodology and application, Atmos. Chem. Phys., 10, 7017-7039,
520   10.5194/acp-10-7017-2010, 2010.
       Lawrence, M., Jöckel, P., and Kuhlmann, R.: What does the global mean OH concentration tell us?, 2001.
       Liu, F., Beirle, S., Zhang, Q., Dörner, S., He, K., and Wagner, T.: NOx lifetimes and emissions of cities and power plants in
       polluted background estimated by satellite observations, Atmos. Chem. Phys., 16, 5283-5298, 10.5194/acp-16-
       5283-2016, 2016.
525   Mann, G., S. Carslaw, K., Spracklen, D., A. Ridley, D., T. Manktelow, P., Chipperfield, M., Pickering, S., and E. Johnson, C.:
       Description and evaluation of GLOMAP-mode: A modal global aerosol microphysics model for the UKCA
       composition-climate model, 2010.
       Manning, M. R., Lowe, D. C., Moss, R. C., Bodeker, G. E., and Allan, W.: Short-term variations in the oxidizing power of the
       atmosphere, Nature, 436, 1001, 10.1038/nature03900
530   https://www.nature.com/articles/nature03900#supplementary-information, 2005.
       McNorton, J., Chipperfield, M., Gloor, M., Wilson, C., Wuhu, F., Hayman, G., Rigby, M., B. Krummel, P., O'Doherty, S., Prinn,
       R., Weiss, R., Young, D., Dlugokencky, E., and Montzka, S. A.: Role of OH variability in the stalling of the global
       atmospheric CH4 growth rate from 1999 to 2006, 1-24 pp., 2016.

Atmospheric
Chemistry
and Physics
Discussions

McPhaden, M. J., Zebiak, S. E., and Glantz, M. H.: ENSO as an Integrating Concept in Earth Science, Science, 314, 1740-1745,
535 10.1126/science.1132588, 2006.
Meng, L., Paudel, R., G. M. Hess, P., and Mahowald, N.: Seasonal and inter-annual variability in wetland methane emissions
  simulated by CLM4Me' and CAM-chem and comparisons to observations of concentrations, 2015.
Miles, G. M., Siddans, R., Kerridge, B. J., Latter, B. G., and Richards, N. A. D.: Tropospheric ozone and ozone profiles retrieved
  from GOME-2 and their validation, Atmos. Meas. Tech., 8, 385-398, 10.5194/amt-8-385-2015, 2015.
540 Monks, S., R. Arnold, S., Hollaway, M., Pope, R., Wilson, C., Wuhu, F., Emmerson, K., J. Kerridge, B., Latter, B., M. Miles, G.,
  Siddans, R., and P. Chipperfield, M.: The TOMCAT global chemical transport model v1.6: Description of chemical
  mechanism and model evaluation, 3025-3057 pp., 2017.
Monks, S. A., Arnold, S. R., and Chipperfield, M. P.: Evidence for El Niño–Southern Oscillation (ENSO) influence on Arctic CO
  interannual variability through biomass burning emissions, Geophysical Research Letters, 39,
545 doi:10.1029/2012GL052512, 2012.
Myhre, G., Shindell, D., Bréon, F.-M., Collins, W., Fuglestvedt, J., Huang, J., Koch, D., Lamarque, J.-F., Lee, D., Mendoza, B.,
  Nakajima, T., Robock, A., Stephens, G., Takemura, T., and Zhang, H.: Anthropogenic and Natural Radiative Forcing,
  in: Climate Change 2013: The Physical Science Basis. Contribution of Working Group I to the Fifth Assessment Report
  of the Intergovernmental Panel on Climate Change, edited by: Stocker, T. F., Qin, D., Plattner, G.-K., Tignor, M.,
550 Allen, S. K., Boschung, J., Nauels, A., Xia, Y., Bex, V., and Midgley, P. M., Cambridge University Press, Cambridge,
  United Kingdom and New York, NY, USA, 659–740, 2013.
Naik, V., Voulgarakis, A., Fiore, A. M., Horowitz, L. W., Lamarque, J. F., Lin, M., Prather, M. J., Young, P. J., Bergmann, D.,
  Cameron-Smith, P. J., Cionni, I., Collins, W. J., Dalsøren, S. B., Doherty, R., Eyring, V., Faluvegi, G., Folberth, G. A.,
  Josse, B., Lee, Y. H., MacKenzie, I. A., Nagashima, T., van Noije, T. P. C., Plummer, D. A., Righi, M., Rumbold, S. T.,
555 Skeie, R., Shindell, D. T., Stevenson, D. S., Strode, S., Sudo, K., Szopa, S., and Zeng, G.: Preindustrial to present-day
  changes in tropospheric hydroxyl radical and methane lifetime from the Atmospheric Chemistry and Climate Model
  Intercomparison Project (ACCMIP), Atmos. Chem. Phys., 13, 5277-5298, 10.5194/acp-13-5277-2013, 2013.
Nisbet, E. G., Dlugokencky, E. J., Manning, M. R., Lowry, D., Fisher, R. E., France, J. L., Michel, S. E., Miller, J. B., White, J. W.
  C., Vaughn, B., Bousquet, P., Pyle, J. A., Warwick, N. J., Cain, M., Brownlow, R., Zazzeri, G., Lanoisellé, M., Manning,
560 A. C., Gloor, E., Worthy, D. E. J., Brunke, E.-G., Labuschagne, C., Wolff, E. W., and Ganesan, A. L.: Rising atmospheric
  methane: 2007–2014 growth and isotopic shift, Global Biogeochemical Cycles, 30, 1356-1370,
  doi:10.1002/2016GB005406, 2016.
Prinn, R. G., Huang, J., Weiss, R. F., Cunnold, D. M., Fraser, P. J., Simmonds, P. G., McCulloch, A., Harth, C., Salameh, P.,
  O'Doherty, S., Wang, R. H. J., Porter, L., and Miller, B. R.: Evidence for Substantial Variations of Atmospheric Hydroxyl
565 Radicals in the Past Two Decades, Science, 292, 1882-1888, 10.1126/science.1058673, 2001.
Randerson, J. T., Van Der Werf, G. R., Giglio, L., Collatz, G. J., and Kasibhatla, P. S.: Global Fire Emissions Database, Version
  4.1 (GFEDv4), in, ORNL Distributed Active Archive Center, 2017.
Rap, A., Scott, C. E., Spracklen, D. V., Bellouin, N., Forster, P. M., Carslaw, K. S., Schmidt, A., and Mann, G.: Natural aerosol
  direct and indirect radiative effects, Geophysical Research Letters, 40, 3297-3301, doi:10.1002/grl.50441, 2013.
570 Rap, A., Richards, N. A. D., Forster, P. M., Monks, S. A., Arnold, S. R., and Chipperfield, M. P.: Satellite constraint on the
  tropospheric ozone radiative effect, Geophysical Research Letters, 42, 5074-5081, doi:10.1002/2015GL064037,
  2015.
Reddington, C. L., Morgan, W. T., Darbyshire, E., Brito, J., Coe, H., Artaxo, P., Marsham, J., and Spracklen, D. V.: Biomass
  burning aerosol over the Amazon: analysis of aircraft, surface and satellite observations using a global aerosol
575 model, Atmos. Chem. Phys. Discuss., 2018, 1-32, 10.5194/acp-2018-849, 2018.
Richards, N. A. D., Arnold, S. R., Chipperfield, M. P., Miles, G., Rap, A., Siddans, R., Monks, S. A., and Hollaway, M. J.: The
  Mediterranean summertime ozone maximum: global emission sensitivities and radiative impacts, Atmos. Chem.
  Phys., 13, 2331-2345, 10.5194/acp-13-2331-2013, 2013.
Riese, M., Ploeger, F., Rap, A., Vogel, B., Konopka, P., Dameris, M., and Forster, P.: Impact of uncertainties in atmospheric
580 mixing on simulated UTLS composition and related radiative effects, Journal of Geophysical Research: Atmospheres,
  117, doi:10.1029/2012JD017751, 2012.
Rigby, M., Prinn, R. G., Fraser, P. J., Simmonds, P. G., Langenfelds, R. L., Huang, J., Cunnold, D. M., Steele, L. P., Krummel, P.
  B., Weiss, R. F., O'Doherty, S., Salameh, P. K., Wang, H. J., Harth, C. M., Mühle, J., and Porter, L. W.: Renewed growth
  of atmospheric methane, Geophysical Research Letters, 35, doi:10.1029/2008GL036037, 2008.
585 Rigby, M., Prinn, R. G., O'Doherty, S., Montzka, S. A., McCulloch, A., Harth, C. M., Mühle, J., Salameh, P. K., Weiss, R. F., Young,
  D., Simmonds, P. G., Hall, B. D., Dutton, G. S., Nance, D., Mondeel, D. J., Elkins, J. W., Krummel, P. B., Steele, L. P.,
  and Fraser, P. J.: Re-evaluation of the lifetimes of the major CFCs and CH_3CCl_3 using
  atmospheric trends, Atmos. Chem. Phys., 13, 2691-2702, 10.5194/acp-13-2691-2013, 2013.
Rossow, W. B., and Schiffer, R. A.: Advances in Understanding Clouds from ISCCP, Bulletin of the American Meteorological
590 Society, 80, 2261-2288, 10.1175/1520-0477(1999)080<2261:Aiucfi>2.0.Co;2, 1999.
Schultz, M. G., Heil, A., Hoelzemann, J. J., Spessa, A., Thonicke, K., Goldammer, J. G., Held, A. C., Pereira, J. M. C., and van het
  Bolscher, M.: Global wildland fire emissions from 1960 to 2000, Global Biogeochemical Cycles, 22,
  doi:10.1029/2007GB003031, 2008.

595   Sitch, S., Cox, P. M., Collins, W. J., and Huntingford, C.: Indirect radiative forcing of climate change through ozone effects on
            the land-carbon sink, Nature, 448, 791, 10.1038/nature06059
        https://www.nature.com/articles/nature06059#supplementary-information, 2007.
        Spivakovsky, C. M., Logan, J. A., Montzka, S. A., Balkanski, Y. J., Foreman-Fowler, M., Jones, D. B. A., Horowitz, L. W., Fusco,
            A. C., Brenninkmeijer, C. A. M., Prather, M. J., Wofsy, S. C., and McElroy, M. B.: Three-dimensional climatological
            distribution of tropospheric OH: Update and evaluation, Journal of Geophysical Research: Atmospheres, 105, 8931-
600   8980, doi:10.1029/1999JD901006, 2000.
        Spracklen, D. V., Jimenez, J. L., Carslaw, K. S., Worsnop, D. R., Evans, M. J., Mann, G. W., Zhang, Q., Canagaratna, M. R., Allan,
            J., Coe, H., McFiggans, G., Rap, A., and Forster, P.: Aerosol mass spectrometer constraint on the global secondary
            organic aerosol budget, Atmos. Chem. Phys., 11, 12109-12136, 10.5194/acp-11-12109-2011, 2011.
        Stevenson, D. S., Johnson, C. E., Collins, W. J., Derwent, R. G., and Edwards, J. M.: Future estimates of tropospheric ozone
605   radiative   forcing   and   methane   turnover — The   impact   of   climate   change,   27,   2073-2076,
            doi:10.1029/1999GL010887, 2000.
        Szopa, S., Hauglustaine, D. A., and Ciais, P.: Relative contributions of biomass burning emissions and atmospheric transport
            to carbon monoxide interannual variability, Geophysical Research Letters, 34, doi:10.1029/2007GL030231, 2007.
        Tilmes, S., Lamarque, J.-F., Emmons, L., Conley, A., G. Schultz, M., Saunois, M., Thouret, V., Thompson, A., Oltmans, S.,
610   Johnson, B., and Tarasick, D.: Ozonesonde climatology between 1995 and 2009: Description, evaluation and
            applications, 28747-28796 pp., 2011.
        van der Werf, G. R., Randerson, J. T., Collatz, G. J., Giglio, L., Kasibhatla, P. S., Arellano, A. F., Olsen, S. C., and Kasischke, E. S.:
            Continental-Scale Partitioning of Fire Emissions During the 1997 to 2001 El Niño/La Niña Period, Science, 303, 73-
            76, 10.1126/science.1090753, 2004.
615   van der Werf, G. R., Randerson, J. T., Giglio, L., van Leeuwen, T. T., Chen, Y., Rogers, B. M., Mu, M., van Marle, M. J. E., Morton,
            D. C., Collatz, G. J., Yokelson, R. J., and Kasibhatla, P. S.: Global fire emissions estimates during 1997–2016, Earth
            Syst. Sci. Data, 9, 697-720, 10.5194/essd-9-697-2017, 2017.
        Voulgarakis, A., Naik, V., Lamarque, J. F., Shindell, D. T., Young, P. J., Prather, M. J., Wild, O., Field, R. D., Bergmann, D.,
            Cameron-Smith, P., Cionni, I., Collins, W. J., Dalsøren, S. B., Doherty, R. M., Eyring, V., Faluvegi, G., Folberth, G. A.,
620   Horowitz, L. W., Josse, B., MacKenzie, I. A., Nagashima, T., Plummer, D. A., Righi, M., Rumbold, S. T., Stevenson, D.
            S., Strode, S. A., Sudo, K., Szopa, S., and Zeng, G.: Analysis of present day and future OH and methane lifetime in the
            ACCMIP simulations, Atmos. Chem. Phys., 13, 2563-2587, 10.5194/acp-13-2563-2013, 2013.
        Voulgarakis, A., and Field, R. D.: Fire Influences on Atmospheric Composition, Air Quality and Climate, Current Pollution
            Reports, 1, 70-81, 10.1007/s40726-015-0007-z, 2015.
625   Voulgarakis, A., Marlier, M. E., Faluvegi, G., Shindell, D. T., Tsigaridis, K., and Mangeon, S.: Interannual variability of
            tropospheric trace gases and aerosols: The role of biomass burning emissions, Journal of Geophysical Research:
            Atmospheres, 120, 7157-7173, doi:10.1002/2014JD022926, 2015.
        Wang, J. S., McElroy, M. B., Logan, J. A., Palmer, P. I., Chameides, W. L., Wang, Y., and Megretskaia, I. A.: A quantitative
            assessment of uncertainties affecting estimates of global mean OH derived from methyl chloroform observations,
630   Journal of Geophysical Research: Atmospheres, 113, doi:10.1029/2007JD008496, 2008.
        Wild, O.: Modelling the global tropospheric ozone budget: exploring the variability in current models, Atmos. Chem. Phys.,
            7, 2643-2660, 10.5194/acp-7-2643-2007, 2007.
        Wolter, K., and Timlin, M.: Monitoring ENSO in COADS with a seasonally adjusted principal component index, 17th Climate
            Diagnostics Workshop, Norman, OK, 1993, 52-57.
635   Wolter, K., and Timlin, M. S.: Measuring the strength of ENSO events: How does 1997/98 rank?, Weather, 53, 315-324,
            doi:10.1002/j.1477-8696.1998.tb06408.x, 1998.
        Wolter, K., and Timlin, M. S.: El Niño/Southern Oscillation behaviour since 1871 as diagnosed in an extended multivariate
            ENSO index (MEI.ext), International Journal of Climatology, 31, 1074-1087, doi:10.1002/joc.2336, 2011.
        Young, P. J., Archibald, A. T., Bowman, K. W., Lamarque, J. F., Naik, V., Stevenson, D. S., Tilmes, S., Voulgarakis, A., Wild, O.,
640   Bergmann, D., Cameron-Smith, P., Cionni, I., Collins, W. J., Dalsøren, S. B., Doherty, R. M., Eyring, V., Faluvegi, G.,
            Horowitz, L. W., Josse, B., Lee, Y. H., MacKenzie, I. A., Nagashima, T., Plummer, D. A., Righi, M., Rumbold, S. T., Skeie,
            R. B., Shindell, D. T., Strode, S. A., Sudo, K., Szopa, S., and Zeng, G.: Pre-industrial to end 21st century projections of
            tropospheric ozone from the Atmospheric Chemistry and Climate Model Intercomparison Project (ACCMIP), Atmos.
            Chem. Phys., 13, 2063-2090, 10.5194/acp-13-2063-2013, 2013.
645   Zhu, Q., Peng, C., Ciais, P., Jiang, H., Liu, J., Bousquet, P., Li, S., Chang, J., Fang, X., Zhou, X., Chen, H., Liu, S., Lin, G., Gong, P.,
            Wang, M., Wang, H., Xiang, W., and Chen, J.: Interannual variation in methane emissions from tropical wetlands
            triggered by repeated El Niño Southern Oscillation, Global Change Biology, 23, 4706-4716, doi:10.1111/gcb.13726,
            2017.